

Article

Facile Synthesis and Characterization of Two Dimensional SnO₂-Decorated Graphene Oxide as an Effective Counter Electrode in the DSSC

Mohamed S. Mahmoud ^{1,2}, Moaded Motlak ³ and Nasser A. M. Barakat ^{1,*}¹ Chemical Engineering Department, Minia University, El-Minia 61111, Egypt; msmm122@yahoo.com² Collage of Applied Science, Department of Engineering, Sohar 311, Oman³ Department of Physics, Collage of Science, University of Anbar, Al Ramadi 31001, Iraq;

moaaed.motlak@yahoo.com

* Correspondence: nasbarakat@minia.edu.eg; Tel.: +20-8623234008

Received: 1 December 2018; Accepted: 22 January 2019; Published: 1 February 2019



Abstract: SnO₂-decorated graphene oxide (SnO₂/GO) was synthesized by the modified Hummers's method, followed by a chemical incorporation of SnO₂ nanoparticles. Then, the nanocomposite was used as an non-precious counter electrode in a dye-sensitized solar cell (DSSC). Although GO has a relatively poor electrical conductivity depending essentially on the extent of the graphite oxidation, presence of SnO₂ enhanced its structural and electrochemical properties. The Pt-free counter electrode exhibited a distinct catalytic activity toward iodine reduction and a low resistance to electron transfer. Moreover, the decorated GO provided extra active sites for reducing I₃[−] at the interface of the CE/electrolyte. In addition, the similarity of the dopant in the GO film and the fluorine-doped tin oxide (FTO) substrate promoted a strong assimilation between them. Therefore, SnO₂-decorated GO, as a counter electrode, revealed an enhanced photon to electron conversion efficiency of 4.57%. Consequently, the prepared SnO₂/GO can be sorted as an auspicious counter electrode for DSSCs.

Keywords: dye sensitized solar cell; SnO₂-decorated graphene oxide; counter electrode; solar energy

1. Introduction

Basically, the conversion of solar energy into electricity proceeds through direct or indirect routes. Currently, direct conversion of solar radiation-to-electricity is receiving the maximum attention. In this regard, silicon-based photovoltaic cell (PV panel) is the most widely used. However, PV cells are suffering from high fabrication cost (\$/kW) because their function counts on the presence of a relatively thick layer of doped silicon to obtain an acceptable photon capture rate. Comparably, the dye sensitized solar cell (DSSC) provides a low-cost transfer route of photons to electrons, due to its superior advantages over the traditional PV cells; it absorbs more solar radiation per surface area than the traditional PV cells [1,2]. Recently, the efficiency of the DSSCs has been increased to 17%, which puts it in the market race with the conventional PV [3]. Mainly, the DSSC consists of a porous layer of titanium oxide nanoparticle coated with a solar sensitive organometallic dye, the counter electrode (Pt), and the working electrolyte (e.g., the redox couple I₃[−]/I[−]). Its mechanism of work is discussed in details elsewhere [4,5]. Numerous efforts to enhance the solar energy-to-electricity efficiency of the DSSCs have been reported. These attempts focused on optimizing the properties of the four components of the DSSC:

1. The sensitized dye
2. The material of the photoanode
3. The redox couple electrolyte and

4. The non-precious counter electrode

In this regard, there have been several attempts to develop stable solar-sensitive dyes [3,6] and electrolytes [6,7]. Similarly, developing the photoanode has been investigated by altering the type of the mesoporous film that is coated over the photo anode glass, such as TiO₂ nanofibers [8,9], ZnO and ZnO/TiO₂ nanocomposite [10,11], SnO₂ [12,13], or CdO [14]. These oxides are mixed with the organometallic dye to form the photoanode of the DSSC.

Compared to the photoanode, the counter electrode (CE) is more expensive because it is usually fabricated from precious metals (e.g., Pt), which adds an additional capital cost. Therefore, developing effective counter electrode from cheap materials can strongly enhance the DSSC's rank. Typically, the CE should assure three attributes [15]: (i) As a catalyst, it should transfer the electron to the oxidized redox couple (I⁻). (ii) As a cathode, it should collect the electrons coming from the outside circuit and get them ready to be transferred to the cell. (iii) As a mirror, it should reflect the transmitted light back to the DSSC to enhance the use of photons [16]. The main characteristics of the optimal CE are summarized as follows [17]: high catalytic activity, high electrical conductivity, maximum reflectivity, low-cost, large surface area, porous nature, optimal thickness, electrochemical and mechanical stability, energy level that matches the potential of the redox couple electrolyte, and high adhesivity with the FTO [17]. As a heterogeneous catalytic reaction is taking place on the surface of the counter electrode, the reduction of the electrolyte (e.g., iodine ion) can be considered a combination of adsorption and electrochemical reaction processes. Accordingly, to exploit their high adsorption capacity, carbon nanomaterials such as nanotubes [18], graphene [19], and nanofibers [20] have been utilized as support for the counter electrode materials. Moreover, some carbonaceous nanostructures show a distinguished activity individually [21,22]. Graphene is branded by its amazing electrical and mechanical properties. Therefore, many researchers show interest in using this nanomaterial in different applications [23]. However, its high hydrophobicity negatively affects the performance in the aqueous media due to the poor contact which adds an additional resistance to the reactants transfer. On the other hand, due to possessing oxygenated groups on the surface, graphene oxide (GO) is more hydrophilic than graphene. However, the newly added active groups decrease the electrical conductivity of GO compared to graphene. The conductivity of GO depends on the C/O ratio in the sample. During the oxidation step, the sp² carbons are removed and replaced by sp³ ones having oxygen functionalities. This process creates a band gap by pulling the bands apart. Hence, when graphene is fully oxidized, the bands are far apart, and the GO behaves as an insulator. In the middle of this fully oxidized GO and pure graphene, it behaves as a semiconductor. Partially oxidized GO shows the appearance of sp³ regions and sp² regions [24], and the GO can conduct through these sp² regions via Klein tunneling [24]. In addition, insertion of a transition metal oxide in the GO layers could play a crucial role in enhancing the electron conduction of the GO. SnO₂ is a crucial semiconductor that is used as a transparent conducting oxide (TCO). This TCO normally coated over the glass substrate and used for optical applications. Hitherto, SnO₂ is usually considered as an oxygen-deficient n-type semiconductor [25]. Therefore, doping GO with SnO₂ nanoparticles may enhance the conductive properties of the GO and promote the electron transfer to the redox chattel in the DSSC. Even though there are intensive studies on alternatives of counter electrode, thus far, to our best knowledge, there is no report regarding the application of SnO₂-decorated GO as counter electrode in the DSSC. In this work, we report the synthesis of SnO₂-decorated GO, its characterization, and application as a counter electrode in the DSSC.

2. Results and Discussion

Figure 1a shows the transmission electron microscope (TEM) image of the prepared material. It is noticeable that the sample composed of a sheet of GO contains randomly distributed nanoparticles. High resolution TEM (HR-TEM) image shown in Figure 1b affirms that the attached nanoparticles appear as textured crystalline mode, which indicates that these nanoparticles are SnO₂-based, highly crystalline compound. However, the distribution of these nanoparticles is random. The higher

magnification image indicates that the interlayer distance is 0.26 nm and the particle size is less than 20 nm.

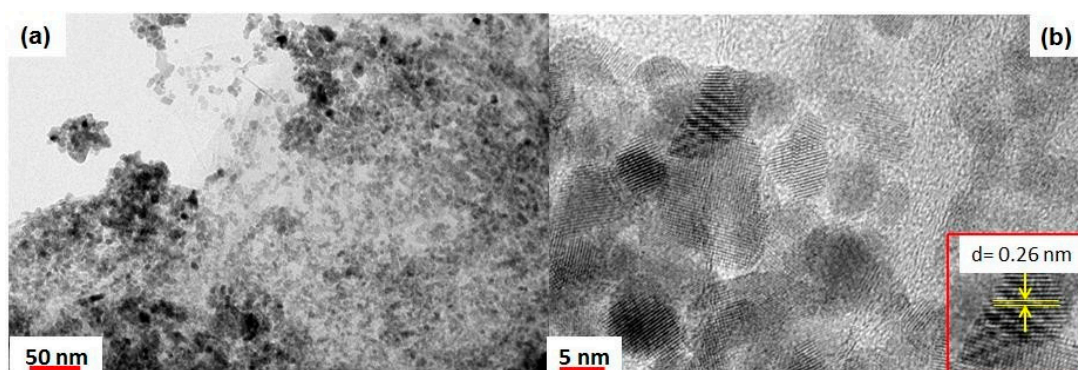


Figure 1. Transmission electron microscope (TEM) (a); and High resolution TEM (HR-TEM) (b) images of SnO₂-incorporated GO.

Figure 2 displays the X-ray diffraction (XRD) patterns of both pristine and decorated GO. Initially, from XRD pattern, it is easy to confirm the formation of GO from the utilized precursor. Typically, the graphite reveals a sharp peak in the XRD pattern at 2θ value of $\sim 26^\circ$. Due to exfoliation, the graphite-identified peak disappears and another peak is formed at $\sim 10^\circ$, while graphene is distinguished by a very broad peak centered at $\sim 24^\circ$ [26]. As shown, the GO main peak at 2θ values of 10.2° , corresponding to the (001) basal plane of GO with a d-spacing value of ($d_{001} = 0.961$ nm), appears in both samples. However, the intensity of such peak in the SnO₂/GO sample has a lower intensity than pure GO. Typically, the intensity of the GO main identification peak is 867 and 1957 count/s for the SnO₂/GO and pristine GO, respectively. The reason of low peak intensity is probably due to the heat treatment and incorporation of foreign atoms in the GO layer, which was also noticed by R. Krishna et al. [27]. In addition, the strong diffraction peaks at 2θ values of 26.38° , 33.48° , 37.76° , and 51.46° corresponding to (110), (101), (200) and (211) crystal planes (JCPDS:41-1445), respectively, confirm the incorporation of tetragonal crystals of SnO₂ inside the GO layer. It is also noticeable that the SnO₂ peaks are broadened, indicating the presence of small crystalline size. It is important to determine the crystal structure of the SnO₂-decorated GO due to its direct effect on the power conversion efficiency of the DSSC. According to Scherrer's equation ($\tau = K\lambda/\beta\cos\theta$, where τ is the ordered (crystalline) domains mean size, λ is the wavelength of the utilized X-ray irradiation (0.1504 nm), K is a constant value with a typical value of 0.9 referring to the shape factor, β is the line broadening at half the maximum intensity (FWHM) in radians and θ is the Bragg angle), the average grain size was determined to be 5.1 nm.

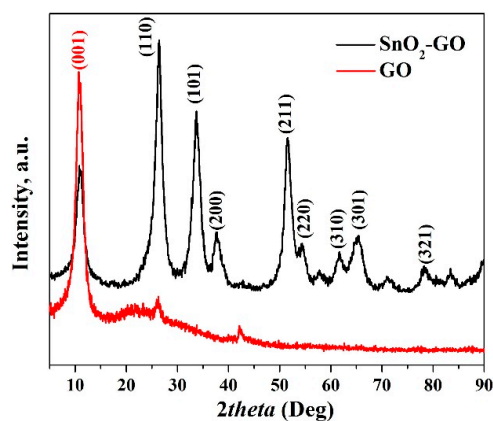


Figure 2. XRD patterns for the pristine and SnO₂-incorporated graphene oxide.

Figure 3 displays the Raman spectra of pristine and SnO₂-incorporated GO in the range of 100–3000 cm⁻¹. In the GO spectrum, two protuberant peaks corresponding to D and G bands, the characteristic peaks of GO, are located at 1354 and 1591 cm⁻¹ with respective I_D/I_G intensities ratio of 1.07. The inset confirms the stability of the prepared GO during the achieved GO decoration process by SnO₂ nanoparticles. As shown in the inset, there is no considerable change in the I_D/I_G intensities ratio. Moreover, in the Raman spectrum, the pristine graphene reveals an additional peak (2D), indicating an increase in the average size of sp² domains at ~2790 cm⁻¹ [28]. As shown, the 2D peak does not appear in the SnO₂-GO spectrum, which confirms maintaining the composition of the GO. In other words, the utilized treatment process did not affect the content of the oxygenated groups covering the surface of GO sheets. The crystalline structure of SnO₂ is a tetragonal rutile with point group D_{4h} [29]. Typically, three modes identifying SnO₂ can be found in the Raman spectrum: 474 cm⁻¹ (E_g), 631 cm⁻¹ (A_{1g}) and 775 cm⁻¹ (B_{2g}) [30]. When the particle size decreases, A_{1g} and B_{2g} modes of SnO₂ are shifted to lower wave numbers and E_g mode is shifted to higher wave number [30]. The obtained results show peaks at 615, 435, 245, and 120 cm⁻¹. The band at 435 cm⁻¹ probably corresponds to the (E_g) mode of the oxide. Similarly, the mode at 615 cm⁻¹ can be assigned to symmetric O-Sn-O stretching (A_{1g}) shifts due to the relatively small particle size of SnO₂ nanoparticles. The position and the intensity of SnO₂ peak in the Raman spectrum depends on the crystal size. The vibrational mode (B_{1g}) peak appears only along with nanomaterials. Thus, in the Raman spectrum, the presence of a peak at 120 cm⁻¹ is associated with non-degenerated B_{1g} mode of SnO₂ and its appearance is caused by lowering the surface phonon frequencies that leads to increase in the inter-atomic distance on the surface [30].

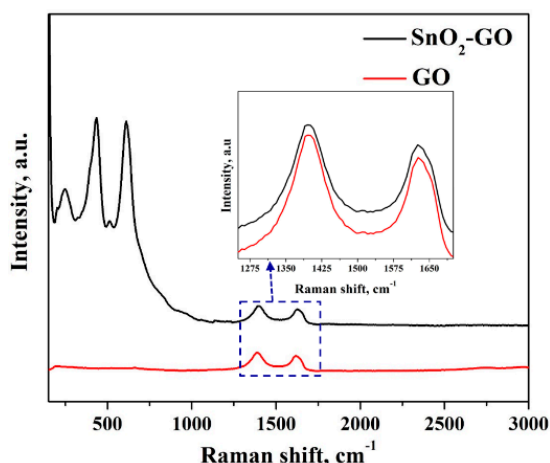


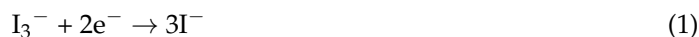
Figure 3. Raman spectroscopy analyses for the pristine and SnO₂-decorated graphene oxide. The inset displays high magnification of the D and G bands.

Overall, based on the aforementioned analytical technique, it is safe to claim that the proposed material is GO sheets decorated by small and highly crystalline SnO₂ nanoparticles.

It is worth mentioning that the function of the redox shuttle (I₃⁻/I⁻) is very important to ensure a stable transfer of electrons between the photoanode and the counter electrode of a DSSC. The photon-induced excitation of the dye leads to transfer of electrons to the oxide semiconductor. Then, the electron donor (I₃⁻) must rapidly return the excited dye back to its ground state. Afterwards, the electron acceptor (I⁻) should move to the CE to get the missing electrons to regenerate the electron donor (I₃⁻). The electron migration through the external circuit will close the circuit [2,4].

To verify the electrocatalytic activity of the as-prepared SnO₂-incorporated GO, cyclic voltammetry (CV) analysis of the prepared catalyst was achieved using a conventional three-electrode system. SnO₂-doped GO, Pt wire and Ag/AgCl served as working, counter and reference electrodes, respectively. The electrolyte solution consisted of 10 mM LiI, 1 mM I₂, and 0.1 M LiClO₄ in acetonitrile. Figure 4a shows the cyclic voltammograms (CV) at scan rate of 25 mV/s. It is clear

that the introduced SnO₂/GO shows both oxidation and reduction peaks, which indicate achieving the following reactions [20].



The counter electrode exhibits high redox current densities, indicating that the speed of the redox reaction on the surface of the modified GO is fast. Besides the activity of the SnO₂ nanoparticles attached on the surface of the GO, the enhancement in the surface area after the decoration process can be assigned as a second reason for the observed high performance. Typically, the measured surface area of the pristine and decorated GO was 159.7 ± 2 and 210.5 ± 3 m²/g, respectively. The increase in the surface area can be attributed to the high exfoliation rate upon addition of the tin precursor. Therefore, the improved specific surface area of the modified GO can be considered as a stimulator for such boost of the electrocatalytic activity toward the reduction of I₃[−] ions. Incidentally, the modified GO is responsible for the efficient reduction of I₃[−] ions by providing sufficient superficial area and promoting fast electronic transformation, which results in higher J_{sc} and solar-electrical conversion efficiency in the DSSC.

Figure 4b illustrates CV curves of the SnO₂-incorporated GO electrode in the prepared electrolyte solution at different scan rates (10–50 mV/s). It is clear that altering the scan rate increased the current density values. In addition, it slightly shifted the potential peaks of the anodic and cathodic reactions. The inset of Figure 4b shows the influence of the scan rate on the anodic and cathodic peak currents. It is noticeable that they are linearly dependent on the scan rate. Such finding discloses that the rate of diffusion of I₃[−] ion is the hindering step in the oxidation–reduction process [20].

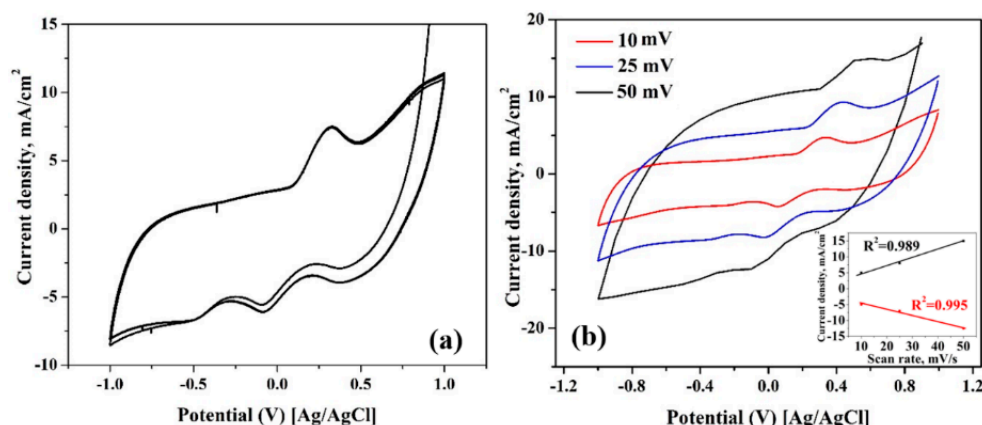


Figure 4. (a) Cyclic voltammety analyses of the introduced SnO₂/GO in presence of iodine solution with a scan rate of 25 mV/s in the potential range from −1 to 1 V vs. Ag/AgCl; and (b) the cyclic voltammograms at different scan rates.

Performing the electrochemical impedance spectroscopy (EIS) analysis of a DSSC helps to get insight about some important performance parameters, such as charge transport through the photoanode and near the counter electrode, charge transfer due to electron back reaction, and capacitive accumulation of the charges at different processes in the cell. It was used to measure the resistances of the individual interfaces of the fabricated DSSC based on the introduced SnO₂/GO counter electrode. The merit of EIS spectrum over the I–V curve is that EIS indicates the response of the solar-induced current on the electrical bias voltage values, which cannot be indicated through the I–V curve.

The impedance spectrum of a DSSC typically shows three semicircles in the Nyquist plot. According to the direction of decreasing frequency, the first semicircle corresponds to the charge transfer processes which happens in the CE/electrolyte interface with a characteristic frequency ω_{CE} ; the second or middle semicircle corresponds to the diffusion of the electron through the TiO₂ layer and the reversible electron reaction with the oxidized state of the redox species at the TiO₂/electrolyte

boundary; and the third semicircle at the low frequency region corresponds to the diffusion of I_3^- in the electrolyte, with a characteristic frequency ω_D [31]. The characteristic frequency for electron transport or diffusion (ω_d) appears in the middle semicircle at the high frequency region, while the peak frequency (ω_k) of that semicircle corresponds to the electron reversible reaction. Figure 5 shows the Nyquist and Bode plots of GO and SnO₂/GO as counter electrodes in the DSSC. In the case of GO, as shown in Figure 5A, only one semicircle appears, indicating an insignificant charge transfer at the GO/electrolyte interface. For the SnO₂/GO plot, two semicircles signify two different kinds of impedance. In the high-frequency region (10^3 – 10^6 Hz), the semicircle denotes the resistance due to the charge transfer (R_{CE}) at the counter electrode/electrolyte interface. In the middle-frequency (1 – 10^3 Hz) region, the semicircle denotes the diffusion through the TiO₂ layer and electron reversible reaction with the oxidized state of the redox species at the TiO₂/electrolyte boundary (R_{CT}). However, in the low-frequency region (0.1 – 1 Hz), no semicircle of the complete response appears, which could be attributed to the small distance between the working and counter electrodes and the low viscosity of the electrolyte.

These data indicate that the low (R_{CE}) is related to a comparatively high rate of electron transfer at the interface of electrolyte/counter electrode, which leads to improve the catalytic activity toward the redox couple in the electrolyte. In the DSSC cell, the (R_{CE}) value was found to be 43.1Ω , which indicates that the SnO₂/GO revealed an effective catalytic activity toward the reduction of I_3^- ions in redox electrolyte. Moreover, the cell shows low series resistance (R_s) value of 23.6Ω , which is attributed to an excellent conductivity of SnO₂/GO film and strong contact between the film and FTO substrate [20].

The catalytic activity of the SnO₂-incorporated GO counter electrode can be presented using current density (J), which is calculated from the charge transfer resistance (R_{CT}) [32]:

$$R_{CT} = RT/nFJ \quad (3)$$

where R is the gas constant ($J/mol \cdot K$), T is temperature (K), n is the number of involved electrons ($n = 2$), and F is the Faraday constant.

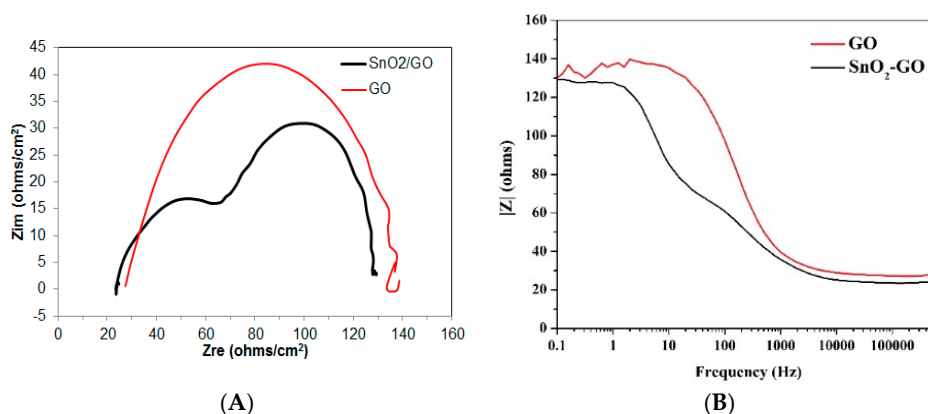


Figure 5. Electrochemical impedance of the DSSC fabricated with GO and SnO₂-incorporated GO-based counter electrode: (A) Nyquist plot; and (B) Bode diagram.

Figure 6 depicts the J – V curves of DSSCs under metal halide lamp illumination. Table 1 displays the photovoltaic parameters from J – V curves and a brief comparison with other counter electrodes. The data indicate that the cell based on the introduced SnO₂/GO exhibited an energy conversion efficiency of 4.57%, which is slightly lower than the standard Pt counter electrode. Such energy conversion efficiency of the cell is linked to the activity of the counter electrode, which synergizes the reduction reaction at the interface of electrolyte/counter electrode, which in turn assists the regeneration of the ground state of the organometallic dye at the interface of electrolyte/photoanode. As shown in Table 1, the other parameters for the fabricated cell are V_{oc} of 0.67 V, J_{sc} of 14.04 mA^{-2}

cm and FF of 0.49. These results are lower than those reported from GO–Pt composite fabricated by low-temperature electrodeposition process, which revealed an energy conversion efficiency of 7.05% [33]. However, the authors used Pt precious metal, which is not aligned with our goals.

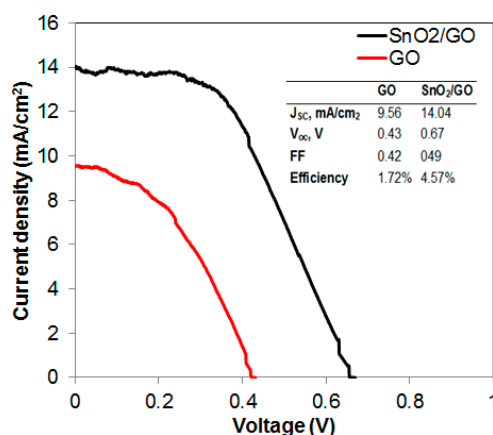


Figure 6. Photovoltaic characteristics (J–V) of fabricated DSSCs using SnO₂-incorporated GO based counter electrode measured under the irradiance of AM 1.5 G sunlight of 100 mW cm^{−2}.

Table 1. The detailed photovoltaic parameters from J–V curves and a brief comparison with other works.

Type of CE	η , %	FF	V _{OC} , V	J _{sc} , mA/cm ²	Ref.
Pt layer	5.9	0.51	0.718	16.12	[20]
CoS/rGO	9.39	0.63	0.764	19.42	[34]
Mw-Pt NPs@GO	7.96	0.71	0.7	16.02	[35]
GO/FTO	3.99	0.38	0.71	14.02	[36]
GO-ED Pt/FTO	7.05	0.66	0.71	14.98	[37]
POMA-FGO (1%)	7.26	0.61	0.73	16.31	[38]
CuS5/FTO5 μ m	1.12	0.52	0.37	5.81	[39]
SnO ₂ /GO	4.57	0.49	0.67	14.04	This study

3. Materials and Methods

3.1. Catalyst Preparation

To prepare the electrode, all the involved chemicals, e.g., SnCl₂, thiourea, graphite, and KMnO₄, were obtained from Sigma Aldrich Co., Seoul, South Korea. The procedure started with slowly dissolving 0.42 g of tin chloride in 20 mL distilled water. Parallely, 0.15 g of thiourea were also dissolved in 20 mL distilled water individually for 20 min. Then, the two solutions were mixed using a magnetic stirrer for 1 h. The GO was prepared by a modified Hummers's method. The next step was to disperse 0.2 g of GO in 100 mL distilled water, and then ultra-sonication for 40 min. Afterwards, the two mixtures were mixed for 20 min, and then 200 mL of hydrazine were added just before the hydrothermal step. Next, hydrothermal treatment was done for 10 h at 180 °C. Finally, the sample was filtered and dried at 60 °C overnight.

3.2. The DSSC Fabrication

The fabrication of DSSCs consisted of three steps [18,39]: fabrication of the photoanode, fabrication of the counter electrode and the addition of the working electrolyte. Typically, FTO substrate glass (FTO 10 Ω /sq.) was used to prepare the photoanode. Preparation started by plating nanocrystalline TiO₂ (Degussa P-25) thin film over FTO glass by simple doctor blade technique. The prepared photoanode had an active area of 0.25 cm² with the film thickness of 8–10 μ m. Then, the FTO was annealed at 450 °C for 30 min. Afterwards, the photoanodes were immersed in the dye solution consisting of

0.3 mM ruthenium(II) 535 bis-TBA (N-719, Solaronix; Sigma, Seoul, South Korea), rinsed with ethanol and dried for 24 h under nitrogen flow. Similarly, the SnO₂-decorated GO was pasted over the FTO glass by simple doctor blade technique. The obtained film was cleaned by ethanol and then dried at 60 °C for 30 min. To complete the fabrication of DSSC, the SnO₂-decorated GO counter electrode was placed over the dye-adsorbed TiO₂ photoanode and sealing was made using Surlyn sheet (SX 1170-60, Solaronix, 60 μm thick) between the two electrodes. Finally, the electrolyte, consisting of lithium iodide (LiI 0.5 M), Iodine (I₂ 0.05 mM), and tetra-butyl-pyridine (C₉H₁₃N 0.2 M) in acetonitrile, was inserted into the holes in the counter electrode using a syringe.

3.3. Characterization and Application

The TEM images of the prepared catalyst were retrieved using JEOL JEM 2010 transmission electron microscope, working at a voltage of 200 kV, (JEOL Ltd., Tokyo, Japan). Clarification of the distance of the TEM images was acquired by ImageJ 1.47v software. To determine the crystal structure of the prepared catalyst, Rigaku X-ray diffractometer (XRD, Rigaku, Tokyo, Japan) with Cu Kα ($\lambda = 1.5406 \text{ \AA}$) was utilized. The Raman spectrum was also acquired using Dispersive Raman spectrometer (BRUKER-SENTERRA, Boerdestr, Warstein, Germany) equipped with an integral microscope (Olympus, Tokyo, Japan). The excitation source was neodymium-doped yttrium aluminum garnet (Nd/YAG) laser (532 nm), and providing a power of 20 mW on the sample, and analyzed by X-ray Diffraction Microanalysis (XPRT-PRO-P-Analysis, The Woodlands, TX, USA). The electrochemical impedance spectroscopy (EIS) and cyclic Voltammetry (CV) measurements were performed using a VersaSTAT 4 (AMETEK, New York, NY, USA) electrochemical analyzer using a conventional three-electrode cell structure. In the utilized cell, glassy carbon, Pt and Ag/AgCl served as working, counter and reference electrodes, respectively. To deposit the proposed GO-based material on the active surface of the working electrode, 2 mg of the function material were added to 20 μL Nafion solution (5 wt %) and 400 μL isopropanol. Afterwards, the suspension was subjected to ultra-sonication process for 20 min. Then, 15 μL of the suspension were poured in three steps on the electrode active area. Finally, the electrode was dried at 80 °C. Current–voltage characteristics of DSSCs were measured by using digital Multimeters (Model 2000, Keithley, Filderstadt, Germany) and a variable load. As a simulation of the solar radiation, a 1000 W metal halide lamp served as a light source, and its light intensity (or radiant power) was adjusted to simulate mornign. Then, 1.5 radiation at 100 mW cm⁻² with a Si photo detector fitted with a KG-5 filter (Schott, Cheney, KS, USA) as a reference was calibrated at NREL (New York, NY, USA). The metal uptake, during the decoration process, was determined by estimating the remaining tin ions in the initial solution using the titration procedure. Briefly, the solution was hot treated with hydrochloric acid, and then drops of starch indicator solution were added. Finally, the solution was titrated against iodate–iodide standard solution. The uptake was determined to be around 15 wt %.

4. Conclusions

SnO₂ nanoparticles-decorated graphene oxide can be synthesized by hydrothermal treatment of GO prepared by Hummers's method in presence of tin chloride. The active chemical groups covering the prepared GO upon using the chemical route lead to a homogeneous distribution for the metallic nanoparticles. Moreover, these groups procure to a good attachment of the inorganic oxide with the carbonaceous support. The prepared SnO₂/GO catalyst improves the electrocatalytic activity toward iodine redox reaction. Moreover, a decrease in the electron transfer was observed due to the harmony between the metallic nanoparticles in the proposed composite and the tin oxide existing in the utilized transparent glass electrodes (FTO). Accordingly, exploiting the prepared catalyst as a counter electrode in the DSSC showed a relatively good energy conversion with an efficiency of 4.57%. Overall, it can be claimed that the SnO₂-decorated GO might be a new effective counter electrode for DSSCs.

Author Contributions: M.S.M. helped in writing the original draft of the manuscript. M.M. helped in the formal analysis. N.A.M.B. helped in supervision and project administration.

Acknowledgments: The authors deeply thank M. Shaheer Akhtar (Chonbuk National University) for measuring the J–V data.

Conflicts of Interest: The authors declare no conflict of interest.

References

1. Mathew, S.; Yella, A.; Gao, P.; Humphry-Baker, R.; Curchod, B.F.; Ashari-Astani, N.; Tavernelli, I.; Rothlisberger, U.; Nazeeruddin, M.K.; Grätzel, M. Dye-sensitized solar cells with 13% efficiency achieved through the molecular engineering of porphyrin sensitizers. *Nat. Chem.* **2014**, *6*, 242. [[CrossRef](#)] [[PubMed](#)]
2. Ning, Z.; Fu, Y.; Tian, H. Improvement of dye-sensitized solar cells: What we know and what we need to know. *Energy Environ. Sci.* **2010**, *3*, 1170–1181. [[CrossRef](#)]
3. Lee, C.-P.; Li, C.-T.; Ho, K.-C. Use of organic materials in dye-sensitized solar cells. *Mater. Today* **2017**, *20*, 267–283. [[CrossRef](#)]
4. Gong, J.; Sumathy, K.; Qiao, Q.; Zhou, Z. Review on dye-sensitized solar cells (DSSCs): Advanced techniques and research trends. *Renew. Sustain. Energy Rev.* **2017**, *68*, 234–246. [[CrossRef](#)]
5. Sharma, S.; Siwach, B.; Ghoshal, S.; Mohan, D. Dye sensitized solar cells: From genesis to recent drifts. *Renew. Sustain. Energy. Rev.* **2017**, *70*, 529–537. [[CrossRef](#)]
6. Ye, M.; Wen, X.; Wang, M.; Iocozzia, J.; Zhang, N.; Lin, C.; Lin, Z. Recent advances in dye-sensitized solar cells: From photoanodes, sensitizers and electrolytes to counter electrodes. *Mater. Today* **2015**, *18*, 155–162. [[CrossRef](#)]
7. Wu, J.; Lan, Z.; Lin, J.; Huang, M.; Huang, Y.; Fan, L.; Luo, G. Electrolytes in dye-sensitized solar cells. *Chem. Rev.* **2015**, *115*, 2136–2173. [[CrossRef](#)]
8. Mahmoud, M.S.; Akhtar, M.S.; Mohamed, I.M.; Hamdan, R.; Dakka, Y.A.; Barakat, N.A. Demonstrated photons to electron activity of S-doped TiO₂ nanofibers as photoanode in the DSSC. *Mater. Lett.* **2018**, *225*, 77–81. [[CrossRef](#)]
9. Joshi, P.; Zhang, L.; Davoux, D.; Zhu, Z.; Galipeau, D.; Fong, H.; Qiao, Q. Composite of TiO₂ nanofibers and nanoparticles for dye-sensitized solar cells with significantly improved efficiency. *Energy Environ. Sci.* **2010**, *3*, 1507–1510. [[CrossRef](#)]
10. Manthina, V.; Baena, J.P.C.; Liu, G.; Agrios, A.G. ZnO–TiO₂ Nanocomposite Films for High Light Harvesting Efficiency and Fast Electron Transport in Dye-Sensitized Solar Cells. *J. Phys. Chem. C* **2012**, *116*, 23864–23870. [[CrossRef](#)]
11. Yang, M.; Dong, B.; Yang, X.; Xiang, W.; Ye, Z.; Wang, E.; Wan, L.; Zhao, L.; Wang, S. TiO₂ nanoparticle/nanofiber—ZnO photoanode for the enhancement of the efficiency of dye-sensitized solar cells. *RSC Adv.* **2017**, *7*, 41738–41744. [[CrossRef](#)]
12. Basu, K.; Benetti, D.; Zhao, H.; Jin, L.; Vetrone, F.; Vomiero, A.; Rosei, F. Enhanced photovoltaic properties in dye sensitized solar cells by surface treatment of SnO₂ photoanodes. *Sci. Rep.* **2016**, *6*, 23312. [[CrossRef](#)] [[PubMed](#)]
13. Zhang, Y.; Qi, T.; Wang, Q.; Zhang, Y.; Wang, D.; Zheng, W. Preparation of SnO₂/rGO Photoanode and Its Effect on the Property of Dye-Sensitized Solar Cells. *IEEE J. Photovolt.* **2017**, *7*, 399–403. [[CrossRef](#)]
14. Bykkam, S.; Kalagadda, B.; Kalagadda, V.R.; Ahmadipour, M.; Chakra, C.S.; Rajendar, V. Effect of Few-Layered Graphene-Based CdO Nanocomposite-Enhanced Power Conversion Efficiency of Dye-Sensitized Solar Cell. *J. Electron. Mater.* **2018**, *47*, 620–626. [[CrossRef](#)]
15. Thomas, S.; Deepak, T.; Anjusree, G.; Arun, T.; Nair, S.V.; Nair, A.S. A review on counter electrode materials in dye-sensitized solar cells. *J. Mater. Chem. A* **2014**, *2*, 4474–4490. [[CrossRef](#)]
16. Wu, J.; Li, Y.; Tang, Q.; Yue, G.; Lin, J.; Huang, M.; Meng, L. Bifacial dye-sensitized solar cells: A strategy to enhance overall efficiency based on transparent polyaniline electrode. *Sci. Rep.* **2014**, *4*, 4028. [[CrossRef](#)] [[PubMed](#)]
17. Wu, J.; Lan, Z.; Lin, J.; Huang, M.; Huang, Y.; Fan, L.; Luo, G.; Lin, Y.; Xie, Y.; Wei, Y. Counter electrodes in dye-sensitized solar cells. *Chem. Soc. Rev.* **2017**, *46*, 5975–6023. [[CrossRef](#)] [[PubMed](#)]
18. Prasetio, A.; Subagio, A.; Purwanto, A.; Widiyandari, H. Dye-sensitized solar cell based carbon nanotube as counter electrode. *AIP Conf. Proc.* **2016**, *1710*, 030054.

19. Hung, K.-H.; Li, Y.-S.; Wang, H.-W. Dye-sensitized solar cells using graphene-based counter electrode. In Proceedings of the 12th IEEE Conference on Nanotechnology (IEEE-NANO), Birmingham, UK, 20–23 August 2012; pp. 1–12.
20. Motlak, M.; Barakat, N.A.; Akhtar, M.S.; Hamza, A.; Kim, B.-S.; Kim, C.S.; Khalil, K.A.; Almajid, A.A. High performance of NiCo nanoparticles-doped carbon nanofibers as counter electrode for dye-sensitized solar cells. *Electrochim. Acta* **2015**, *160*, 1–6. [[CrossRef](#)]
21. Lee, W.J.; Ramasamy, E.; Lee, D.Y.; Song, J.S. Efficient dye-sensitized solar cells with catalytic multiwall carbon nanotube counter electrodes. *ACS Appl. Mater. Int.* **2009**, *1*, 1145–1149. [[CrossRef](#)]
22. Wang, X.; Zhi, L.; Müllen, K. Transparent, conductive graphene electrodes for dye-sensitized solar cells. *Nano Lett.* **2008**, *8*, 323–327. [[CrossRef](#)] [[PubMed](#)]
23. Marcaccio, M.; Paolucci, F. *Making and Exploiting Fullerenes, Graphene, and Carbon Nanotubes*; Springer: Berlin, Germany, 2014.
24. Gao, W. The chemistry of graphene oxide. In *Graphene Oxide*; Springer: Berlin, Germany, 2015; pp. 61–95.
25. Rahal, A.; Benramache, S.; Benhaoua, B. Preparation of n-type semiconductor SnO₂ thin films. *J. Semicond.* **2013**, *34*, 083002. [[CrossRef](#)]
26. El-Deen, A.G.; Barakat, N.A.; Khalil, K.A.; Kim, H.Y. Development of multi-channel carbon nanofibers as effective electrosorptive electrodes for a capacitive deionization process. *J. Mater. Chem. A* **2013**, *1*, 11001–11010. [[CrossRef](#)]
27. Krishna, R.; Titus, E.; Okhay, O.; Gil, J.C.; Ventura, J.; Ramana, E.V.; Gracio, J.J. Rapid electrochemical synthesis of hydrogenated graphene oxide using Ni nanoparticles. *Int. J. Electrochem. Sci.* **2014**, *9*, 69.
28. Wei, A.; Wang, J.; Long, Q.; Liu, X.; Li, X.; Dong, X.; Huang, W. Synthesis of high-performance graphene nanosheets by thermal reduction of graphene oxide. *Mater. Res. Bull.* **2011**, *46*, 2131–2134. [[CrossRef](#)]
29. Katiyar, R.; Dawson, P.; Hargreave, M.; Wilkinson, G. Dynamics of the rutile structure. III. Lattice dynamics, infrared and Raman spectra of SnO₂. *J. Phys. C Solid Stat. Phys.* **1971**, *4*, 2421. [[CrossRef](#)]
30. Li, Z.; Shen, W.; Zhang, X.; Fang, L.; Zu, X. Controllable growth of SnO₂ nanoparticles by citric acid assisted hydrothermal process. *Colloid Surf. Physicochem. Eng. Asp.* **2008**, *327*, 17–20. [[CrossRef](#)]
31. Sarker, S.; Ahammad, A.J.S.; Seo, H.W.; Kim, D.M. Electrochemical Impedance Spectra of Dye-Sensitized Solar Cells: Fundamentals and Spreadsheet Calculation. *Int. J. Photoenergy* **2014**, *2014*, 17. [[CrossRef](#)]
32. Murakami, T.N.; Grätzel, M. Counter electrodes for DSC: Application of functional materials as catalysts. *Inorg. Chim. Acta* **2008**, *361*, 572–580. [[CrossRef](#)]
33. Yu, Y.-H.; Teng, I.J.; Hsu, Y.-C.; Huang, W.-C.; Shih, C.-J.; Tsai, C.-H. Covalent bond-grafted soluble poly(o-methoxyaniline)-graphene oxide composite materials fabricated as counter electrodes of dye-sensitized solar cells. *Org. Electron.* **2017**, *42*, 209–220. [[CrossRef](#)]
34. Huo, J.; Wu, J.; Zheng, M.; Tu, Y.; Lan, Z. High performance sponge-like cobalt sulfide/reduced graphene oxide hybrid counter electrode for dye-sensitized solar cells. *J. Power Sources* **2015**, *293*, 570–576. [[CrossRef](#)]
35. Demir, E.; Savk, A.; Sen, B.; Sen, F. A novel monodisperse metal nanoparticles anchored graphene oxide as Counter Electrode for Dye-Sensitized Solar Cells. *Nano-Struct Nano-Obj.* **2017**, *12*, 41–45. [[CrossRef](#)]
36. Jang, H.-S.; Yun, J.-M.; Kim, D.-Y.; Na, S.-I.; Kim, S.-S. Transparent graphene oxide–Pt composite counter electrode fabricated by pulse current electrodeposition-for dye-sensitized solar cells. *Surf. Coat. Technol.* **2014**, *242*, 8–13. [[CrossRef](#)]
37. Satoshi, K.; Daiki, A.; Etsuo, S.; Masahiro, M. Copper Sulfide Catalyzed Porous Fluorine-Doped Tin Oxide Counter Electrode for Quantum Dot-Sensitized Solar Cells with High Fill Factor. *Int. J. Photoenergy* **2017**, *2017*, 5461030.
38. Zaaba, N.; Foo, K.; Hashim, U.; Tan, S.; Liu, W.-W.; Voon, C. Synthesis of graphene oxide using modified hummers method: Solvent influence. *Procedia Eng.* **2017**, *184*, 469–477. [[CrossRef](#)]
39. Rao, S.S.; Gopi, C.V.; Kim, S.-K.; Son, M.-K.; Jeong, M.-S.; Savariraj, A.D.; Prabakar, K.; Kim, H.-J. Cobalt sulfide thin film as an efficient counter electrode for dye-sensitized solar cells. *Electrochim. Acta* **2014**, *133*, 174–179.

